Optimization of OLED Microcavity Design and Fabrication for Light Field Display

Jordan Peckham, Jiaqi Cheng, Andrew Ward, Jennifer Campbell, Katie Krause, Danny Bachman, Steve Rutledge, Tushar Biswas, Arash Mohammadpour and Wally Haas
Avalon Holographics
St. John's, NL, Canada

Abstract
Control of the emission characteristics of a light source in a light field display poses a significant benefit in the resulting 3D display quality. The design of microcavity OLEDs is detailed, including FDTD optimizations. The resulting output profiles for the microcavity OLEDs are compared to standard OLEDs and the designs.

Keywords
Light field display; 3d display; microcavity; OLED

1. INTRODUCTION
A test to determine if a display meets the window to the world criteria, known as the 3D version of the Turing test [1], inquiring if a user can distinguish the 3D scene geometry perceived with a light field display from the geometry perceived when viewing the real world has been formulated [2]. The display passes this test if the viewer cannot distinguish the display from reality. For a display to meet this criteria it should provide strong 3D perceptual cues; stereo, motion parallax and focus cues, all the while providing a high resolution image [3].

Current light field displays, which provide multiple views such that at each viewing position a user will get a separate view in each eye, provide an interesting experience, but suffer from some limitations. In particular, the individual views must be separated in such a way that the user experiences smooth transitions between viewing zones, while maintaining an independent and perceivable view from the adjacent views. Therefore, the ability to control the emission characteristics of each unit of the light field display is desired, in particular with an increased pixel density to provide an increased resolution per view.

The path to creating a 3D display that mimics the real world includes decreasing source dimensions. Inorganic light emitting diodes (LED) are not suitable for miniaturization into the submicron regime due to several obstacles including fabrication challenges and quantum confinement related changes in band structure. Organic light emitting diodes (OLED), on the other hand, present a possible alternative because their amorphous structure is not bound by quantum confinement [4]. In addition, OLEDs with sub-100 nm diameters have been fabricated and exhibit similar performance to larger area OLEDs [5].

Spectral narrowing, intensity enhancement, and emission profile modification of microcavity OLEDs (MCOLED) are a well reported result of the spontaneous emission of planar microcavity devices. The three main design variables affecting the performance of a microcavity are the reflectance of the top and bottom surfaces, and the optical path length. Therefore, by specifically fixing the distance between the reflective surfaces, attaining a high reflectance value for one of the mirrors, and finely controlling the reflectance of the opposing mirror, the output of each OLED can be finely tuned. In this report, the cathode functions as both bottom reflective surface in the microcavity structure, as well as the base electrical contact. The upper reflective surface is comprised of a series of alternating high and low refractive index dielectric layers known as a distributed Bragg reflector (DBR). The DBR is selected to allow tailoring of the output parameters, since the refractive index properties of the constituent materials and the number of pairs of the dielectric layers change the peak reflectance and reflectance profile of the dielectric layered mirror. Moreover, the DBR has the additional benefit of having no absorption in the visible spectrum.

In this paper, the development and results of microcavity based OLEDs are detailed. The theoretical design variables used to define the initial structure of the OLEDs at the peak emission wavelength are summarized. FDTD simulations used to optimize the optical path lengths in the microcavity are detailed. Fabricated MCOLED results are presented, and compared to OLEDs not bound in a microcavity, as well as FDTD simulation results.

2. BACKGROUND
An organic light emitting diode consists of multiple organic material layers, between a pair of electrodes, resulting in characteristic broad spectral width and Lambertian intensity profile emission. While these emission characteristics may be desirable for standard display solutions, the ability to tailor the optical properties of the device for a light field display using microcavity effects is required. A perspective view of a microcavity based OLED is shown in Figure 1.

When a light emitting material is placed between two reflective surfaces, the spontaneous-emission photon density of states is redistributed, resulting in an enhancement of emission intensity in the perpendicular direction as well as in narrowing of the emission spectra [6]. This enhancement occurs when the total optical path length, L_i, satisfies the relationship

$$L_i = \frac{m\lambda_i}{2} \tag{1}$$

where m is a positive integer, commonly referred to as the mode of the microcavity, and λ_i is wavelength of peak emission from the cavity [7].

Emission Characteristics
The reduced angular spread due to the microcavity can be approximated as

$$\delta\theta_{FWHM} = \sqrt{\frac{2\lambda_i(1-\sqrt{R_{Cathode}R_{DBR}})}{\pi L_i \sqrt[4]{R_{Cathode}R_{DBR}}}} \tag{2}$$

and similarly the FWHM of the output spectrum is determined as

$$\delta\lambda_{FWHM} = \frac{\lambda_i^2(1-\sqrt{R_{Cathode}R_{DBR}})}{2\pi L_i \sqrt[4]{R_{Cathode}R_{DBR}}} \tag{3}$$

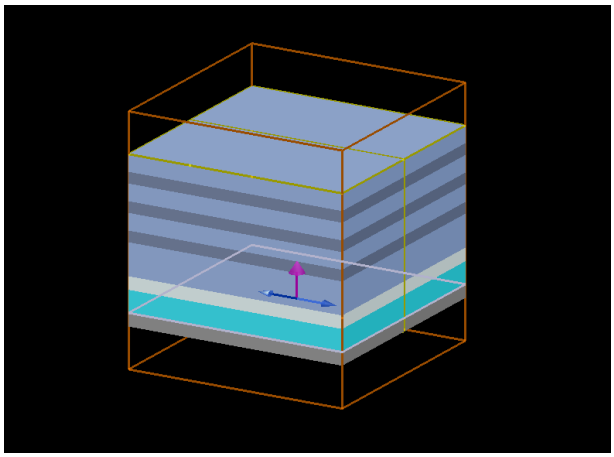

Figure 1: Perspective view of a single MCOLED stack from FDTD simulation.

where $R_{Cathode}$ is the reflectance of the cathode, and R_{DBR} is the reflectance of the DBR [8].

Distributed Bragg Reflector

The highest reflectance of the DBR structure is attained when the layer thicknesses, d_i, are chosen such that the optical path length of each layer is one quarter of the resonance wavelength, or

$$L_j = \frac{\lambda_{Bragg}}{4} \tag{4}$$

where λ_{Bragg} is the design wavelength for the DBR [9]. Under these conditions, all reflections will add in phase, and the transmission will decrease exponentially as a function of mirror thickness. The reflectance of a DBR at λ_{Bragg} can be approximated as

$$R_{DBR} = \left(\frac{1 - (n_1/n_2)^{2\Lambda}}{1 + (n_1/n_2)^{2\Lambda}} \right)^2. \tag{5}$$

where n_1 is the refractive index of the low index DBR material at λ_{Bragg}, n_2 is the refractive index of the high index DBR material at λ_{Bragg}, and Λ is the number of dielectric pairs [10]. At longer or shorter wavelengths, the reflections begin to add out of phase, therefore the total reflections decrease [8]. The result is a broadband high-reflectance region centered on λ_{Bragg}, referred to as the stop band, $\delta\lambda_{stopband}$, determined as

$$\delta\lambda_{stopband} = \frac{2\lambda_{Bragg}(n_2 - n_1)}{\pi \cdot n_{eff}} \tag{6}$$

where n_{eff} is the effective index [11].

Optical Path Length

The total optical path length of the microcavity is represented as

$$L_i = L_{DBR} + L_{Organics} + L_{Cathode}, \tag{7}$$

the sum of the penetration depth into the DBR, L_{DBR}, the total optical path length in the OLED materials, $L_{Organics}$, and the penetration depth into the metal cathode, $L_{Cathode}$. The optical path length in the materials between the two reflective surfaces is found as the sum of the optical path lengths in each material,

$$L_{Organics} = \sum_{i}^{N} n_i d_i \tag{8}$$

where n_i and d_i are the layer indices and thicknesses, respectively. The penetration depth into the DBR can be determined as [12, 13]

$$L_{DBR} = \frac{\lambda_{Bragg}}{2} \frac{n_{eff}}{n_2 - n_1}, \tag{9}$$

and the penetration depth into the metal cathode is

$$L_{Cathode} = \left| \frac{\Phi_m}{4\pi} \lambda_i \right| \tag{10}$$

where Φ_m is the phase shift at the metal reflector, given by

$$\Phi_m = \tan^{-1} \left(\frac{2\, n_{Cavity}\, k_{Cathode}}{n_{Cavity}^2 - n_{Cathode}^2 - k_{Cathode}^2} \right) \tag{11}$$

where n_{Cavity} is the refractive index of the material in contact with the cathode, and $n_{Cathode}$ and $k_{Cathode}$ are the real and imaginary parts of the refractive index of the metal cathode [12].

3. RESULTS AND DISCUSSION

Design Methodology

For the general MCOLED design, where $\lambda_{Bragg} = \lambda_i$, the theoretical model presented in the previous section will yield a satisfactory fabrication result. However, when $\lambda_{Bragg} \neq \lambda_i$, these equations can only be used to provide an initial approximation of the required MCOLED design. In particular, Equation 9 cannot reliably be used to determine a value for the penetration depth into the DBR at a value other then λ_{Bragg}. The remainder of this section details the design procedure reported here for the case when $\lambda_{Bragg} \neq \lambda_i$. Initially, a series of approximations are used to estimate the path length, and mirror reflectance. An OLED design is specified, containing a set of material thicknesses which are used in Equation 8 to determine the optical path length in the OLED materials. Assuming the same metal cathode is used as in this OLED design as in the microcavity design, the penetration depth can be calculated using Equation 10. The thickness of the cathode is significantly increased in the microcavity design as compared to the OLED design to prevent unwanted transmission. The final step in estimating the optical path length in the microcavity is the penetration into the DBR, which can approximated to be equal to λ_i. Using Equation 1, the minimum mode number, m, can be determined.

Defining the emission characteristics required of the MCOLED will determine the reflectance of the top and bottom mirrors. In the case where a metal mirror is used, the reflectance value is bound to an upper limit due to absorption. Using Equation 2 and/or Equation 3, the minimum reflectance for the DBR can be determined. With knowledge of the minimum reflectance, a script created using MATLAB [14] based on a transfer matrix method (described in more detail in Ref. [15]), which determines the reflectance profile, is used. An example of the output of this custom script is shown in both Figures 2 and 3.

Using the final design of the DBR, the penetration depth at the design wavelength for the MCOLED, λ_i, must be determined. Using Lumerical FDTD Solutions, a commercial-grade simulator based on the finite-difference time-domain method [16], the penetration depth is determined by measuring propagation length at λ_i and comparing the result to a discrete mirror. A similar simulation is completed for the metal cathode to validate the calculation using Equation 10. These values can then be used in Equation 7 to define the initial model of the MCOLED.

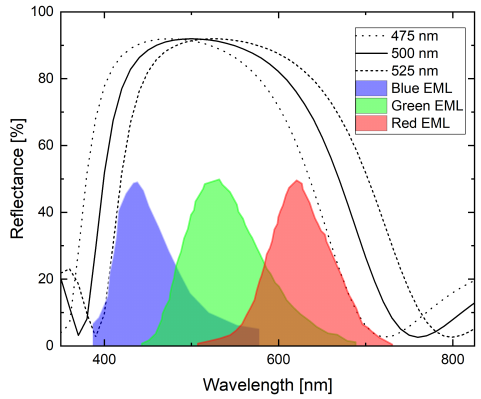

Figure 2: Plot of the theoretical DBR reflectance profiles for Bragg wavelengths of λ_{Bragg} = 475, 500, and 525 nm, plotted with the expected emission profile for a red, green, and blue OLED.

A particle swarm optimization is employed to determine the final MCOLED structure, accounting for the entire wavelength range of the emitting layer in the OLED structure. The Optimizations to determine the required optical path length for each microcavity OLED were created in Lumerical FDTD Solutions, using a custom script to create the MCOLED structure. A perspective of the modeled microcavity OLED stack is shown in Figure 1. The script creates each layer thickness as a variable which can then be optimized by the simulations software. The refractive index and extinction coefficients for each material were initially measured by ellipsometry and/or supplied by the material supplier, and imported into the simulation to ensure accurate results. It should be noted that there are many ways to optimize the structure, including adding a filler layer above the anode structure which can be changed to tune the optical path length, similarly varying the anode thickness can be used, or tuning one or all of the OLED material thicknesses.

Design Example

For the design of a MCOLED, an example of a red OLED where λ_R = 630 nm is considered, in which the overall design contains a DBR which is continuous across RGB sub-pixels, and has λ_{Bragg} = 500 nm.

The reflectance spectrum of the DBR must have a stopband width equivalent to the full output for the red, green, and blue OLEDs. While many materials may be used for a DBR, TiO_2 and SiO_2 have a large refractive index contrast and the deposition of these materials is common and well known. Since the stopband is not evenly distributed around λ_{Bragg}, the refractive index values for SiO_2 and TiO_2 were used in a script based on a transfer matrix model to determine the DBR reflectance profile. The expected emission profile for the RGB OLEDs is shown in Figure 2, beneath the expected reflectance profile for a Λ = 3 DBR with λ_{Bragg} = 475 nm, 500 nm, and 525 nm using TiO_2 and SiO_2, showing that λ_{Bragg} = 500 nm fully distributes the stopband across the RGB OLEDs. Using Equations 5 and 6, noting that the refractive index of SiO_2 and TiO_2 at 500 nm is 1.449 and 2.515, respectively, R_{DBR} = 86.4 % and $\lambda_{stopband}$ = 171 nm, which are similar values found in Figure 2.

The design for the red OLED constitutes 4 materials, with a total optical path length of $L_{Organics}$ = 274.4 nm (Equation 8). From Equation 10, the penetration depth for an Aluminum cathode at λ_R = 630 nm is found to be $L_{Cathode}$ = 21.6 nm. Estimating L_{DBR} = 630 nm, Equation 7 gives L_R = 925.9 nm and m = 3. Note, the thickness of the ITO was set through iterative calculations so the path length was approximately λ_R.

To find the actual penetration depth at λ_R, FDTD is used as described in the previous section. Using a model of the DBR immersed in air, as well as a point monitor and a plane wave source, the accumulated phase for the reflection from the DBR is determined. Calculating the phase accumulation for the reflection from an ideal metallic reflector ($\phi = 2\pi d/\lambda$), the phase change in the DBR can be calculated, from which the penetration depth can be determined. For λ_R, the penetration depth in the DBR is determined to be 658 nm.

Using L_{DBR} = 658 nm, for m = 3, the optical path length in the microcavity has to be reduced, or if m = 4 the material(s) thickness must be increased to satisfy Equation 1. Since the ITO is variable in this design example, reduction of the ITO thickness by 15 nm decreases $L_{Organics}$ to 263.4 nm, resulting in an m = 3 mode of 629 nm.

With an initial design for λ_R defined, the MCOLED structure can be defined in Lumerical FDTD solution. The simulation is created using a custom script, created in Lumerical's scripting language, adding the functionality to vary each material thickness individually during parameter sweeps or optimizations. In this case, the thickness of the ITO is the varied quantity, with a figure of merit (FOM) defined as the maximum electric field intensity at λ_R. The resulting spectrum of the optimizations is plotted with the experimentally measured MCOLED results in Figure 4b.

Experimental Results

To confirm the transfer matrix model script, a 3 period DBR on silicon was fabricated, shown in Figure 3. The measured reflectance profile of the resulting DBR is plotted against the theoretically determined profile, showing very good agreement. The resulting stopband width is determined to be approximately 240 nm, with a maximum reflectance over 98%.

The resulting spectral output for a green and red OLED with a microcavity are shown in Figure 4, respectively. The spectral output for the OLEDs was recorded using an Ocean Optics STS spectrometer. The FWHM values for each curve are determined by fitting a Gaussian function to the collected data and calculating

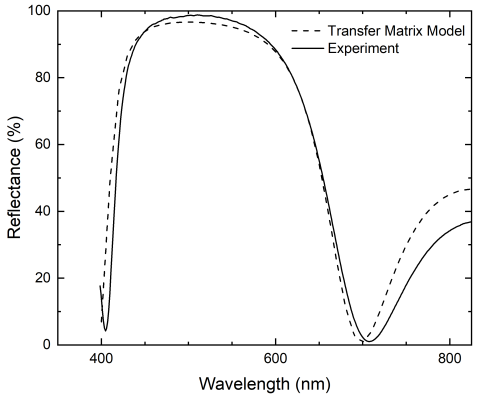

Figure 3: Plot of the measured and theoretical reflectance spectrum of a Λ = 3 DBR fabricated on silicon.

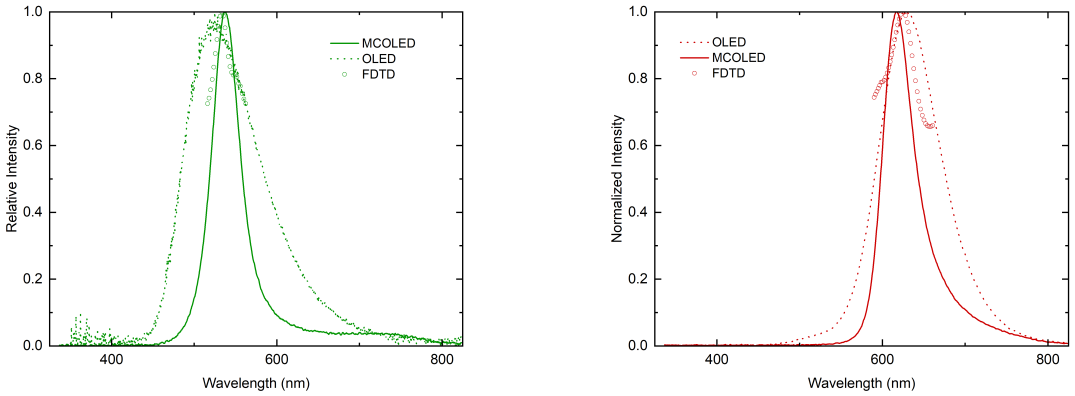

(a) (b)

Figure 4: Comparison of spectral output of a standard OLED, microcavity based OLED, and FDTD optimization results for a) a Green OLED, where the FWHM for the MCOLED is 40.4 nm, and for the standard OLED is 101.6 nm, and b) a Red OLED with a FWHM for the MCOLED is 46.7 nm, and for the standard OLED is 87.0 nm.

the FWHM. The green OLED shows a FWHM reduction of over 2.5 times, reducing from an 101.6 nm to 40.4 nm. Similarly, the FWHM is reduced nearly 2 times, from 87.0 nm to 46.7 nm. From the design example presented in this report, the resulting emission spectrum of the optimized MCOLED is plotted in Figure 4b (open circles). The simulation result shows good agreement with the measured MCOLED emission spectrum, with a small shift in the peak emission. This is likely due to a difference in a layer, or multiple layers thickness or refractive index during the fabrication of the MCOLED.

4. CONCLUSIONS

An introduction to the design equations to determine the optical path length, and estimate the output profiles were presented. Details of the FDTD simulations to optimize the optical path lengths were reported, and the resulting output spectrum of the fabricated OLEDs is compared with the modeled structures.

5. REFERENCES

[1] A. Turing, "Computing machinery and intelligence," Mind, vol. 59, no. 236, pp. 433–460, 1950.

[2] M. S. Banks, D. M. Hoffman, J. Kim, and G. Wetzstein, "3D Displays," Annual Review of Vision Science, vol. 2, no. 1, pp. 397–435, 2016.

[3] J. Geng, "Three-Dimensional display technologies," Advances in Optics and Photonics, vol. 5, no. 2, p. 131, 2013.

[4] J. G. C. Veinot, H. Yan, S. M. Smith, J. Cui, Q. Huang, and T. J. Marks, "Fabrication and properties of organic light-emitting â^nanodiodeâ^ arrays," Nano Letters, vol. 2, no. 4, pp. 333–335, 2002.

[5] H. Yamamoto, J. Wilkinson, J. P. Long, K. Bussman, J. A. Christodoulides, and Z. H. Kafafi, "Nanoscale organic light-emitting diodes," Nano Letters, vol. 5, no. 12, pp. 2485–2488, 2005. PMID: 16351200.

[6] A. B. Djurišić and A. D. Rakić, "Organic microcavity light-emitting diodes with metal mirrors: dependence of the emission wavelength on the viewing angle," Appl. Opt., vol. 41, pp. 7650–7656, Dec 2002.

[7] B. Masenelli, A. Gagnaire, L. Berthelot, J. Tardy, and J. Joseph, "Controlled spontaneous emission of a tri(8-hydroxyquinoline) aluminum layer in a microcavity," Journal of Applied Physics, vol. 85, no. 6, pp. 3032–3037, 1999.

[8] G. Björk, Y. Yamamoto, and H. Heitmann, Spontaneous Emission Control in Semiconductor Microcavities, pp. 467–501. Boston, MA: Springer US, 1995.

[9] H. Sugawara, K. Itaya, and G. ichi Hatakoshi, "Hybrid-type ingaalp/gaas distributed bragg reflectors for ingaalp light-emitting diodes," Japanese Journal of Applied Physics, vol. 33, no. 11R, p. 6195, 1994.

[10] C. W. Wilmsen, H. Temkin, and L. A. Coldren, Vertical-Cavity Surface-Emitting Lasers. July 1999.

[11] M. S. Skolnick, T. A. Fisher, and D. M. Whittaker, "Strong coupling phenomena in quantum microcavity structures," Semiconductor Science and Technology, vol. 13, no. 7, p. 645, 1998.

[12] A. Dodabalapur, L. J. Rothberg, R. H. Jordan, T. M. Miller, R. E. Slusher, and J. M. Phillips, "Physics and applications of organic microcavity light emitting diodes," Journal of Applied Physics, vol. 80, no. 12, pp. 6954–6964, 1996.

[13] S. Tokito, T. Tsutsui, and Y. Taga, "Microcavity organic light-emitting diodes for strongly directed pure red, green, and blue emissions," Journal of Applied Physics, vol. 86, no. 5, pp. 2407–2411, 1999.

[14] MATLAB, version 9.3.0 (R2017b). Natick, Massachusetts: The MathWorks Inc., 2018.

[15] H. MacLeod and H. Macleod, Thin-Film Optical Filters, Fourth Edition. Series in Optics and Optoelectronics, CRC Press, 2010.

[16] Lumerical, "FDTD solutions, ver. 8.18.1365," 2017.